3D ultrastructural organisation of calcium release units in the avian sarcoplasmic reticulum

DOI:
10.1242/jeb.197640

Document Version
Accepted author manuscript

First posted online on 27 February 2019 as 10.1242/jeb.197640
Access the most recent version at http://jeb.biologists.org/lookup/doi/10.1242/jeb.197640

3D ultrastructural organisation of calcium release units in the avian sarcoplasmic reticulum

Thomas M. D. Sheard[1]^, Sanjay R. Kharche[1,2,3], Christian Pinali[1] and Holly A. Shiels[1]*

[1]University of Manchester, Faculty of Biology, Medicine and Health, Oxford Road, Manchester, M13 9PL, United Kingdom

[2]Department of Medical Biophysics, University of Western Ontario, London, N6A 3K7, Canada

[3] Lawson Health Research Institute, 800 Commissioners Road East, London, Ontario, N6C 2R5, Canada

Corresponding authors:

*Holly Shiels, CTF Building, Grafton Street, Manchester M13 9PL, UK.
holly.shiels@manchester.ac.uk (Holly A. Shiels);

^Thomas Sheard, present address: University of Leeds, Garstang Building, Woodhouse Lane, Leeds, LS2 9JT, UK. tommichaelsheard@gmail.com (Thomas M. D. Sheard)

Keywords: bird, chicken, computational model, calcium diffusion, electron tomography, peripheral coupling

Summary statement: We used electron tomography to create 3D reconstructions of calcium release units in the avian heart. We combined measurements with computer modelling to infer structure-function relationship pertinent to excitation-contraction coupling.

Abbreviations

Ca^{2+} - calcium / CRU - calcium release unit / SR - sarcoplasmic reticulum / PC - peripheral coupling / cSR - corbular SR / LTCC - L-type calcium channel / RyR - ryanodine receptor / jSR - junctional SR / CICR - calcium-induced calcium release / EjSR - extended junctional SR / ET - electron tomography / TEM - transmission electron microscopy / fSR - free SR / LA - left atrium / RA - right atrium / LV - left ventricle / RV - right ventricle

Abstract

Excitation-contraction coupling in vertebrate hearts is underpinned by calcium (Ca^{2+}) release from Ca^{2+} release units (CRUs). CRUs are formed by clusters of channels called ryanodine receptors on the sarcoplasmic reticulum (SR) within the cardiomyocyte. Distances between CRUs influence the diffusion of Ca^{2+}, thus influencing the rate and strength of excitation-contraction coupling. Avian myocytes lack T-tubules, thus Ca^{2+} from surface CRUs (peripheral couplings, PCs), must diffuse to internal CRU sites of the corbular SR (cSR) during centripetal propagation. Despite this, avian hearts achieve higher contractile rates and develop greater contractile strength than many mammalian hearts, which have T-tubules to provide simultaneous activation of the Ca^{2+} signal through the myocyte. We used 3D electron tomography to test the hypothesis that the intracellular distribution of CRUs in the avian heart permits faster and stronger contractions despite the absence T-tubules. Nearest edge-edge distances between PCs and cSR, and geometric information including surface area and volumes of individual cSR, were obtained for each cardiac chamber of the White Leghorn chicken. Computational modelling was then used to establish a relationship between CRUs distances and cell activation time in the avian heart. Our data suggest that cSR clustered close together along the Z-line is vital for rapid propagation of the Ca^{2+} signal from the cell periphery to the cell centre which would aid in the strong and fast contractions of the avian heart.

1. Introduction

The four-chambered avian heart possesses many similarities to its mammalian counterpart. Both groups independently evolved a fully divided ventricle, capable of producing fast contractile rates with robust pressure development. However, despite similarities in cardiac performance and gross organ morphology, there are substantial differences on a cellular and subcellular level within the cardiomyocytes. Avian atrial and ventricular myocytes are long (>100 µm) and thin (3-9 µm), with a small cross-sectional area (~56 μm^2) and cell volume (~10 pL); these features provide a large surface area to volume ratio (Akester, 1981; Bogdanov *et al.*, 1995; Dzialowski and Crossley II, 2015). It is likely that these morphological features allow excitation-contraction coupling to work within the necessary timescale without sarcolemmal invaginations, known as T-tubules (Sommer and Johnson, 1969). T-tubules are found in all mammalian ventricular myocytes and in atrial myocytes of large mammals, and are important for synchronised depolarisation in these larger cells (Dibb *et al.*, 2009). The lack of T-tubules, characteristic of ectothermic vertebrates (fish, amphibians and non-avian reptiles), has been associated with slower heart rates and less robust contractile function (Shiels and Galli, 2014). We hypothesise that the subcellular organization of calcium (Ca^{2+}) release units (CRUs) within the avian myocyte may reconcile this apparent enigma.

Contraction and relaxation of the heart is underpinned by Ca^{2+} cycling in the cardiomyocytes. Following membrane depolarisation, Ca^{2+} enters the cell via voltage-gated L-type Ca^{2+} channels (LTCC). The initial Ca^{2+} that enters via LTCCs induces further Ca^{2+} release from the intracellular stores of the sarcoplasmic reticulum (SR), in a process called Ca^{2+}-induced Ca^{2+} release (CICR). SR Ca^{2+} is released by the ryanodine receptor (RyR) channels, which cluster in structures defined as CRUs. In birds, there are 2 types of CRUs. The first are peripheral couplings (PCs), which are clusters of RyRs on the surface of junctional SR (jSR), directly adjacent to sarcolemmal LTCCs. The second type of CRU is formed by RyR clusters which are not associated with the surface sarcolemma, known as corbular SR (cSR) (also referred to as extended jSR, EjSR). cSR are shorter, rounder segments of SR than those found at the PCs. Despite being positioned micrometres from the sarcolemma (Sommer, 1995), these internal CRUs contribute to global Ca^{2+} release and are necessary for robust excitation-contraction coupling (Franzini-Armstrong *et al.*, 2005). Ca^{2+} released at PCs must diffuse centripetally to the cSR/EjSR. Ca^{2+} is taken up by contracting myofilaments and adjacent mitochondria, or can be buffered in the cytosol, and thus $[Ca^{2+}]$ falls rapidly the further it travels from a CRU (Sobie *et al.*, 2006). The distribution of CRUs, as well as the depletion of SR Ca^{2+} stores, ensures that excitation-contraction coupling is not endlessly regenerative and unstable, a situation that would be pro-arrhythmic and deleterious to the myocyte (Cannell *et al.*, 1995).

There is a limited amount of functional data on Ca^{2+} flux pathways in avian cardiomyocytes. [^{3}H] ryanodine binding studies in pigeon and finch left ventricle (LV) indicate the density of RyRs and the Ca^{2+} sensitivity of RyRs are similar to mammals (Junker *et al.*, 1994). An early study showed a high density of LTCC current and a prominent T-type Ca^{2+} channel current in whole-cell voltage clamped finch ventricular myocytes (Bogdanov *et al.*, 1995), which the authors suggested could aid in CICR in the absence of T-Tubules. This same study reported faster inactivation kinetics of I_{Ca} in finch compared with rat myocytes and suggested that this may facilitate fast heart rates.

We are unaware of studies that quantify the dynamics of avian intracellular Ca^{2+} movement directly (Kim *et al.*, 2000), but it is possible to speculate on this by examining Ca^{2+} cycling in other cells that are similar in structure. Ectotherms, mammalian neonatal cardiomyocytes, and mammalian nodal and Purkinje cells also lack T-tubules and tend to be thinner in diameter than mammalian ventricular cardiomyocytes. Studies from these cell types show that Ca^{2+} levels rise rapidly at the periphery, followed by a time-dependent rise in the cell centre (Boyden *et al.*, 2000; Woo *et al.*, 2003; Shiels and White, 2005; Stuyvers *et al.*, 2005; Louch *et al.*, 2015).

Our current understanding of structural organization of the Ca^{2+} release system in birds discussed above has been characterised using 2D transmission electron microscopy (TEM) (Franzini-Armstrong *et al.*, 1999; Perni *et al.*, 2012). However, a more realistic representation of the CRU distribution in space can be achieved with 3D electron microscopy. In this study we characterise the distribution of CRUs in myocytes from each of the four chambers of the heart of the White Leghorn chicken (*Gallus gallus domesticus*) using electron tomography (ET). This technique enables the reconstruction and visualisation of subcellular organisation of the SR network in a detailed 3D structure. Tomograms from both atria and both ventricles were reconstructed, and the structures of interest were segmented to 1) study the nearest edge-edge distances between PCs and between cSR; and 2) to obtain cSR volumes and surface areas to determine Ca^{2+} capacity and RyR cluster size. These inter-CRU distances were used in to inform a computer model of Ca^{2+} wave dynamics which tested the effect of inter-CRU distances on whole cell Ca^{2+} activation.

2. Methods

2.1 Tissue samples and specimen preparation

Three adult chickens (White Leghorn variety, *Gallus gallus domesticus*; 1.5-2 kg in body mass) were acquired from Hinchliffe's Farm, Huddersfield, UK. White Leghorns are a slow-growing bird, bred for egg production with no pre-disposition to cardiac dysfunction (Mirsalimi *et al.*, 1993). Chickens were transported to the University of Manchester Biological Services Facility where they were humanely euthanised with pentobarbital, followed by dislocation of the neck in accordance with Scientific Procedures Act 1986. Hearts were excised, and tissue from each of the four chambers (left atria, LA; right atria, RA; left ventricle, LV; right ventricle, RV) was cut into 1 mm^3 samples and placed into Karnovsky fixative with $CaCl_2$ (2% formaldehyde, 2.5% glutaraldehyde, 50mM $CaCl_2$, 0.1M HEPES). Tissue preparation was according to the Ellisman protocol (Deerinck *et al.*, 2010). All reagents were obtained from Sigma.

Sectioning was carried out on a Reichert-Jung UltraCut E ultramicrotome using a glass knife. Sections of ~100 nm thickness (gold coloured ribbons) were produced for observation using a FEI Tecnai 12 Bio Twin transmission electron microscope operated at 100 kV to assess tissue preparation prior to electron tomography (ET).

2.2 Electron tomography

Electron tomography (ET) was performed using an FEI Tecnai G2 Polara transmission electron microscope at the University of Manchester Electron Microscopy Facility, operated at 300 kV using magnifications of approximately x10,000, x12,000, and x15,500. For ET, sections of ~400 nm thickness (green/purple coloured ribbons) were collected on 200 mesh grids. 10 nm gold fiducial markers were added to the sections to aid tilt series collection, alignment and data set reconstruction. Tilt series were taken at areas where the myofibrils were longitudinal, as this aids the identification of the cSR. Single-axis tilt series were acquired at 1° intervals from -60° to +60°, or as close to this maximal angle range as possible. Tilt series were obtained from multiple cells within each of the atria and ventricles for all individuals. Alignment, reconstruction and segmentation were performed in the open-source software package *IMOD* (Kremer *et al.*, 1996). *eTomo* was used for alignment and reconstruction, and *3dmod* was used to view the tomograms, segment the structures of interest and to obtain the distances, volumes, and surface area measurements from the 3D reconstructions.

Following manual segmentation, the edge-edge distances between the CRUs were measured. PCs were identified as specialised regions of SR in close apposition (10-15 nm) to the sarcolemma (Junker *et al.*, 1994), while cSR were identified as spherical structures (~100 nm in diameter) attached to the SR network, predominantly found along Z-lines (Asghari *et al.*, 2009). Nearest edge-edge distances between PCs and between cSR were obtained from *IMOD* by drawing a line in the tomogram volume between the segmented CRUs. Nearest edge-to-edge distances are important for understanding cellular Ca^{2+} dynamics as they indicate the minimum distance that must be crossed by Ca^{2+} released at one site in order to act on an adjacent site (Perni *et al.*, 2012). Since cSR are distributed around the Z-lines, we measured distances between cSR distributed around the same Z-line. Geometric data regarding individual cSR were obtained by fully segmenting each cSR in every slice of each tomogram.

2.3 Computational methods

2.3.1. Model geometry

A 2D Ca^{2+} wave model representing an avian cardiomyocyte was constructed to assess the relationship between inter-CRU distances and whole cell Ca^{2+} activation times. The myocyte was constructed as 8 µm wide (Y axis) and 136 µm long (X axis) (Kim *et al.*, 2000). PCs were placed at regular intervals along the cell membrane in the X direction; Z-lines were placed at regular intervals along the X axis and extended across the Y axis, and cSR were placed at regular intervals on the Z-lines (see Fig. 5A). The model geometry was discretised at a space step of 0.05 µm and thus PCs were placed at a depth from the cell membrane of 50 nm. This is greater than the biological distance (~ 10-15 nm) but we were required to accept this limitation due to the computational power required to provide finer discretisation. CRUs were separated by distances d1 (distance between PCs), d2 (distance between Z-lines), d3 (distance between cSR along a Z-line). These distances were varied in a systematic way to encompass the range of values measured in the tomogram datasets. Distance d1 was tested at 0.25, 0.5 and 0.75 µm, d3 at 0.1, 0.2, 0.4, 0.6 µm, and d2 was varied to represent Z-line spacing indicative of a myocyte at rest (1.7-1.9 µm), as well as encompassing values that could be achieved during myocardial stretch (2.1 µm) and myocardial contraction (1.5 µm). The ranges of distances are tabulated in the Table S1.

2.3.2. Ca^{2+} dynamics model

The Ca^{2+} dynamics model was adapted from previous models (Cheng *et al.*, 1993; Smith *et al.*, 1998; Izu *et al.*, 2001). CRU activation began at the surface sarcolemma and moved towards the centre of the cell. Cell membrane activation initiated propagation of the Ca^{2+} wave in the Y direction. At t = 0, $[Ca^{2+}]$ was raised to 100 µM at Y = 0 µm and Y = 8 µm for 1 ms. Ca^{2+} dynamics were then permitted to evolve for the duration of 1 heartbeat (225 ms), according to the equations given in *2.3.3.* Whole cell activation was achieved when all grid locations reached a $[Ca^{2+}]$ value of 100 µM or more at least once (as per Smith *et al.*, 1998; Izu *et al.,* 2001). Ca^{2+} release was simulated as a stochastic process, release at a CRU occurred when local $[Ca^{2+}]$ exceeded 0.1 µM as described previously (Smith *et al.*, 1998). The probability of a given CRU being open was assumed to be proportional to *Jpump* (see below). Once a CRU was open, it was permitted to release Ca^{2+} for 10 ms (Smith *et al.*, 1998). The spatial network of CRUs were diffusively coupled to permit simulation of Ca^{2+} waves (Izu *et al.*, 2001).

The effect of mobile buffers was omitted. This may affect the absolute slope of the relationship between Ca^{2+} activation time and the distances between CRUs, but is not expected to impact the relative effect of changing distance (d1, d2 and d3) on activation time.

Robust implicit finite difference solvers developed previously (Kharche *et al.*, 2017) were used to solve the reaction-diffusion equations using a maximum temporal step of 0.02 ms (Table S1). Ten simulations were performed for each combination of distances (d1, d2, d3), and an average activation time from the 10 simulations was taken to form each data point. Parallelisation was implemented using message passing interface (MPI). Each simulation required 24 processors 4 hours to complete.

2.3.3. Model equations for Ca^{2+} wave propagation simulations.

Model equations were derived from those found in equation 2 of Izu et al (Smith *et al.*, 1998; Izu *et al.*, 2001).

$$\frac{\partial[Ca^{2+}]_i}{\partial t} = D_c \nabla^2 [Ca^{2+}]_i + J_{buffers} + J_{pump} + J_{leak} + J_{ryr} \quad \text{Eq. 1}$$

$$\frac{\partial[CaB_n]}{\partial t} = -J_n \quad \text{(immobile buffers)} \quad \text{Eq. 2}$$

$$J_n = -k_n^{+}[Ca^{2+}]_i([B_n]_{total} - [CaB_n]) + k_n^{-}[CaB_n] \quad \text{Eq. 3}$$

$$J_{pump} = \frac{v^{\max}_{pump}[Ca^{2+}]_i^{m}}{K^{m}_{pump} + [Ca^{2+}]_i^{m}}, \quad m = 3.98 \quad \text{Eq. 4}$$

$$J_{leak} = -J_{pump}(c_\infty) = -\frac{v^{\max}_{pump} c_\infty^{m}}{K^{m}_{pump} + c_\infty^{m}}, \quad c_\infty = 0.1\ \mu M \quad \text{Eq. 5}$$

$$J_{ryr} = O \times \sigma_{ryr} \quad \text{at CRU locations.} \quad \text{Eq. 6}$$

J_{ryr} is the Ca^{2+} released by the CRU, σ_{ryr} is a 10 ms pulse of 2 pA amplitude injected into the medium by the RyR at CRU location. The variable O took values of 1 or 0 depending on whether the CRU was open or not respectively, and was determined stochastically. The probability of O being open was assumed to be proportional to *Jpump*. Once assigned a value of 1, O retained the value for 10 ms, the open time for the CRU (Smith *et al.*, 1998).

2.4 Statistics

Statistics were performed using *GraphPad Prism* with unpaired t-tests and one-way ANOVAs, with Tukey post hoc analysis as specified in the figure legends. The threshold for statistical significance was $P < 0.05$. The results are expressed as mean ± s.e.m., with the number of measurements, from the number of tissues sections and the number of animals, provided in each legend. The spread of data is shown using scatter plots of individual data points with mean values overlaid.

3. Results

3.1 Segmented model for calculating distances

Each tomogram is a reconstruction of an approximately 400 nm thick section of avian cardiac tissue (Fig. 1; Movie S1). When the tissue is sectioned longitudinally with respect to the axis of the cells, it is apparent that cSR (yellow) are localised at the Z-lines and thus are separated at roughly the length of the sarcomere (Fig. 1A,B). The 3D structural model (Fig. 1C; Movie S2) gives a representative display of cSR spread along Z-lines, as well as the entire SR network adjacent to the sarcolemma.

3.1.1 Peripheral couplings

PCs are defined as clusters of RyRs on the surface of the jSR which are directly adjacent (10-15 nm) to LTCCs on the sarcolemma (Fig. 2A,B). The mean (± s.e.m.) nearest edge-edge distances between PCs in each of the four chambers of the heart were as follows: LA 377 ± 19 nm (n=380), RA 347 ± 22 nm (n=228), LV 334 ± 26 nm (n=193), RV 462 ± 30 nm (n=195)(n= number of individual distances measured; Fig. 2C). Distances between PCs in the RV were significantly greater (one-way ANOVA, $P<0.05$) than those measured in the other cardiac chambers.

3.1.2 Corbular sarcoplasmic reticulum

The internal CRUs in avian hearts are the cSR, which are spherical structures of approximately 100 nm diameter, typically found staggered along the Z-line (Fig. 3A,B; Movie S3). cSR are notably larger in size than the network tubules of free SR (fSR), however they are highly polymorphous in their geometry, varying in shape and size (described below). The mean (± s.e.m.) nearest edge-edge distances between cSR at the same Z-line (Fig. 3C) in each of the four chambers of the heart were as follows: LA 423 ± 16 nm (n=286), RA 501 ± 20 nm (n=189), LV 485 ± 24 nm (n=133), RV 465 ± 23 nm (n=194). Distances measured in LA were significantly shorter than in RA but not different from the two ventricles (one-way ANOVA $P<0.05$).

3.2 Geometric models for individual corbular sarcoplasmic reticulum

ET enables the 3D rendering of structures of interest (Fig. 4A,B). Thus diameter (Fig. 4C), surface area (Fig. 4D) and volume (Fig. 4E) of cSR in each chamber of an individual bird heart was measured to provide insight into their role in Ca^{2+} release (Table S2). The scatterplots (Fig. 4C,D,E) highlight the polymorphic nature of the geometry of bird cSR. The LA cSR were smaller (one-way ANOVA $P<0.05$) in volume and surface area than the other chambers.

3.3 Computational modelling Ca^{2+} dynamics

To understand how inter-CRU distances may impact on Ca^{2+} activation time in an avian myocyte devoid of T-tubules, we constructed a spatially extended 2D Ca^{2+} wave model. In the model, CRUs were placed at locations separated by distances d1 (distance between PCs), d2 (distance between Z-lines), d3 (distance between cSR along a Z-line) (Fig. 5A). Frames from a simulation of Ca^{2+} waves show the mode of diffusion across the cell, [Ca^{2+}] initially increasing at the periphery before diffusion into the interior along the z-lines (Fig. 5B).

CRU distances in the model were varied in a systematic way to encompass the range of values measured in the tomograms, in order to deduce the effect on whole cell activation time (Fig. 6). This analysis suggests that distance between PCs (d1) has little effect on whole cell Ca^{2+} activation time (Fig. 6A). In contrast, when the distance between cSR (d3) is increased from 0.1 µm to 0.2 µm, activation time is delayed by approximately 3.5 ms; as d3 is increased to 0.4 µm activation time is more than 10 ms longer than at 0.1 µm (Fig. 6B). At larger d3 distances (beyond those measured between cSR within a Z-line in the current study) activation time is slowed even further. Under these conditions, widely separated PCs (d1) compound the effect and activation time requires approximately 20 ms. In general, activation time is unaffected as distance between Z-lines are varied (d2) in a manner anticipated during sarcomeric stretch and contraction (Fig. 6A,B). Indeed, because the distance d3 was considerably smaller than distance d2, the CRUs along the Z -lines activated prior to Ca^{2+} passively diffusing to neighbouring Z-lines that were not proximal to the PCs.

4. Discussion

Aves occupy a unique position in vertebrate evolution. They possess a 4-chambered heart with a fully divided ventricle, which arose independently from that in mammals. However, despite gross structural similarities to mammalian hearts, at a cellular level, the avian cardiomyocyte more closely resembles that of (non-avian) reptiles. This study is the first to use electron tomography to investigate the subcellular distribution of the intracellular Ca^{2+} release machinery in the avian heart. We measured distances between PCs and between cSR along a Z-line, and found the PCs to be closer together and the cSR further apart than those reported previously using 2D TEM (Franzini-Armstrong *et al.*, 1999; Perni *et al.*, 2012). Our study has also revealed the diversity of the cSR volumes and varied distribution of these structures in all four cardiac chambers. We then used a computational approach to test how varying distances between these subcellular CRUs affects Ca^{2+} activation time. Our model highlights the importance of distances between cSR along a Z-line (d3). Together, our findings suggest that cSR clustered close together along the Z-line are vital for rapid propagation of the Ca^{2+} signal from the cell periphery to the cell centre, and facilitate strong and fast contractions.

4.1 Peripheral couplings distances

CRUs in the form of PCs have been identified in the hearts of all vertebrates studied, except in the frog ventricle, and are most often associated with the Z-lines (Shiels and Galli, 2014). The mean distances between nearest neighbour PCs in the White Leghorn chicken ranged from 334 nm in LV, to 462 nm in RV, which is comparable to previous values measured using 2D TEM in LV (472 nm (Franzini-Armstrong *et al.*, 1999) and 567 nm (Perni *et al.*, 2012)). We found similar distances between PC in

the LV, RA and LA but slightly longer distances in the RV. The functional significance of this pattern is unclear. Size and frequency of peripheral CRUs varies between vertebrate species and between cardiac chambers within a species, and in some studies this variability has been related to the efficacy of excitation-contraction coupling (Perni *et al.*, 2012; Shiels and Galli, 2014). Indeed, animals with high heart rates (i.e. finch and rat, resting heart rate ~300-350 bpm) have closer PCs than animals with slower heart rates (Perni *et al.*, 2012) (i.e. chicken, resting heart rate ~200 bpm; lizard and fish, heart rate dependent on temperature but generally below 120 bpm (Farrell, 1991)). The distances measured in our study supports previous work in chicken (Perni *et al.*, 2012), which suggests PCs are activated by adjacent LTCCs in the sarcolemmal membrane directly, with little spread of activating Ca^{2+} longitudinally between PCs. Indeed, our simulations suggest that changing the distance between PCs between 250 nm and 750 nm has little impact on whole cell activation, particularly when the distances between cSR are narrow (Fig. 6). This differs from mammalian atrial myocytes and from birds with faster heart rates and/or contractile force (i.e. finch (Perni *et al.*, 2012)) where extensive and propagative CICR between neighbouring CRUs at the cell periphery has been observed (Chen-Izu *et al.*, 2006). In the finch heart, closely packed PCs are further aided by higher density of LTCCs (Bogdanov *et al.*, 1995) to achieve fast heart rates.

4.2 Corbular SR distances

The CRUs of the avian cSR can be thought of as Ca^{2+} release relay stations, carrying the wave of Ca^{2+} from the myocyte periphery to the cell centre in the absence of T-tubules. We found the average distance between cSR at the same Z-line to range from 422 nm in LA, to 500 nm in RA, which are significantly larger than those reported by Franzini-Armstrong's group for LV (148 nm (Franzini-Armstrong *et al.*, 1999) and 235 nm (Perni *et al.*, 2012)) using 2D TEM images taken in a transverse section. Franzini-Armstrong et al. state that "larger distances were ignored" in their measurements, so although the exact threshold used for excluding large distances is not specified, it may explain the discrepancy between studies. The heterogeneous distribution of organelles (e.g. mitochondria), combined with changes in distances between organelles during the contraction-relaxation cycle are both features which help prevent circular, endless propagation of a Ca^{2+} wave. Indeed, our computational model indicates that the distance between cSR has a dramatic effect on the activation time. As cSR distances are varied from those measured previously (~150-235 nm) to those measured in our study (~400-500 nm), activation time more than doubles (Fig. 6). Thus, chains of closely distributed cSR at a Z-line increase the probability that Ca^{2+} will be able to diffuse and activate neighbouring units.

4.3 Corbular SR Geometry

We provide the first 3D geometrical description of cSR in chicken hearts. A similar diverse and polymorphic description has been detailed for the jSR and the T-tubule lattice in mouse cardiomyocytes (Hayashi *et al.*, 2009). Average diameters for cSR from each of the four chambers ranged from 120-130 nm, a parameter that aided cSR identification. The average volume of a cSR in each of the four chambers ranged from 446,000 - 600,000 nm^3, but the largest and smallest ranged from 120,000 nm^3 to 1,410,000 nm^3. The average surface area from each of the four chambers ranged from 22,000 to 28,000 nm^2 but the extremes were 9,000 nm^2 and 60,000 nm^2. Thus, there is extreme heterogeneity in the avian cardiomyocyte's Ca^{2+} release structures.

We were unable to resolve individual RyR positions on the cSR in this study. However, given the average surface area of cSR was between 22,000 to 28,000 nm^2, and knowing that a single RyR is 29 x 29 nm^2, or 841 nm^2 (Chen-Izu *et al.*, 2006; Baddeley *et al.*, 2009), we calculate that the average chicken cSR could support between 26-33 RyR molecules. RyRs probably do not occupy the entire cSR surface, for instance the dyad is only partially filled, and RyR clusters often present a checkerboard appearance (Baddeley *et al.*, 2009; Asghari *et al.*, 2014). We therefore estimate the average cSR possesses approximately 13-16 RyRs.

Calculations concerning jSR Ca^{2+} capacity (whereby jSR of volume $7x10^{-4}$ μm^3 contains 21,000 Ca^{2+} ions (Sobie *et al.*, 2002)), lead us to suggest the average avian cSR would contain between 13,380 and 18,000 Ca^{2+} ions. The minimum and maximum volumes of cSR found here, would thus contain 3,600 and 42,300 Ca^{2+} ions respectively. A 1pA current releases around 3,000 ions per millisecond (Sobie *et al.*, 2002), and thus the total capacity of the cSR analysed in this study permits Ca^{2+} release for ~5 ms in total before the SR is depleted of Ca^{2+}. SR Ca^{2+} available for release at these CRUs is replenished by SERCA Ca^{2+} uptake along the fSR network, which diffuses back towards the junctional area containing the RyRs. Thus the total capacity of the cSR does not finitely dictate the duration of Ca^{2+} release. It is likely that the total capacity can be released in the order of tens of milliseconds, correlating with previous measurements for known spark durations (Sobie *et al.*, 2002; Stern *et al.*, 2013) although the actual spark duration in avian cardiomyocytes is not known. These estimates correlate with the Ca^{2+} activation time of our model which ranges between 5 and 25 ms, with mean ~15 ms, for the whole cell to be activated, depending on CRU spacing.

4.4 Ca^{2+} dynamics model

We used a spatially extended 2D cell model to improve the interpretation of our experimental data. The model showed that the variation of distances between cSR within a Z-line supersedes that of distances between PCs at the cell membrane for setting Ca^{2+} activation time of the cell. Our model has limitations that need to be considered when interpreting our results. First, stimulation was assumed to be generated by a rapidly propagating electrical pulse along the length of the cardiomyocyte membrane. Therefore, the initiated Ca^{2+} wave had an inward propagation. Thus, barring any numerical and boundary condition effects, it may be expected that PCs played a limited role in the output of whole cell Ca^{2+} activation. Our model also incorporated local stochastic Ca^{2+} release, or sparks. The Ca^{2+} released by the sparks diffused in the cytoplasm uniformly in all directions; thus the Ca^{2+} diffusing from a cSR would stimulate release from the directly adjacent CRU along the same Z-line prior to stimulating other CRUs. In previous studies, inter-CRU distances were assumed to be uniform in both X and Y direction, thus the work here extends these earlier models (Izu *et al.*, 2001; Izu *et al.*, 2013). However, in our model the locations of the CRUs were assumed to be symmetric, which aligns with the positioning along the Z-lines that we observed experimentally in the bird heart. However, stochasticity in the spatial distribution of CRUs has been observed (Qu *et al.*, 2014), and will be included in future studies. Lastly, due to the limited functional studies of Ca^{2+} dynamics in avian myocytes (Kim *et al.*, 2000), the model was parameterised based on mammalian data. Further functional studies are need to accurately measure Ca^{2+} flux in avian cardiomyocytes. Improved numerical schemes and solvers are also required to permit exploration of the experimental data in more depth. However, peak systolic Ca^{2+} is reached in a similar time frame and at a similar level in our model and that in mammals (Bers, 2002), despite the difference in cell structure between species.

4.5 Perspectives for avian cardiac performance

Domestic chickens have an average heartbeat of 218 beats min^{-1} (Prosheva *et al.*, 2015). A single cardiac cycle is ~0.275 s comprised of the following electrocardiogram components: P wave (atrial depolarisation) ~30 ms, PQ interval ~60 ms (AV-conduction), QRS (ventricular depolarisation) ~30 ms, and QT interval (duration ventricular action potential) ~140 ms (Prosheva *et al.*, 2015). Ca^{2+} release follows the depolarising wave and thus our mean Ca^{2+} activation time of 12-20 ms is within a reasonable range. In the scenario where cSR distances are at or beyond the level we observed in our tomographic data, activation time would be closer to 25-30 ms. However, in vivo the rate of Ca^{2+} removal and SR replenishment will also influence the speed of the calcium cycle, as increase/decrease in heart rate is predominantly dictated by the duration of the interval between T and P waves (Dzialowski and Crossley II, 2015). Functional studies are required in avian myocytes to reveal the complexities of Ca^{2+} signalling in this cell type, for instance the speed of Ca^{2+} extrusion, and specific channel currents.

In birds with faster heart rates, such as the finch or hummingbird, rapid cardiac contraction relies on even faster relaying of the Ca^{2+} signal. This is brought about by closer spacing of CRUs, and in the case of the finch heart, existence of EjSR in place of cSR (Perni *et al.*, 2012). EjSR are more elongated CRUs, which might offer a greater capacity for Ca^{2+} storage, increased numbers of RyRs per cluster for Ca^{2+} release, or a better geometry for the spread of signal to neighbouring sites.

5. Summary

Our measurements of distances between PCs and cSR, coupled with computational simulations, suggest that in chicken cardiomyocytes the Ca^{2+} transient would be initiated at the periphery, be large in concentration around this sub-sarcolemmal space, and diffuse toward the interior along chains of cSR. The resulting effect would be spatial inhomogeneity and nonsynchronous spread of Ca^{2+} across the whole myocyte. However, upon activation of many CRUs, given that Ca^{2+} is of large enough magnitude, diffusion between cSR positioned at adjacent Z-lines is possible, becoming more probable the closer they are to one another. This pattern is similar to that found in neonatal mammalian myocytes (Louch *et al.*, 2015). As noted by others previously (Perni *et al.*, 2012), the extensive and almost exclusive location of cSR along the Z-lines in bird myocytes induces a high degree of refractoriness to longitudinal Ca^{2+} wave propagation, with activation initiated independently at PCs cascading through the cSR. Thus, the organization of CRUs and the short diffusional distance for Ca^{2+} transport in narrow cells allows for strong and fast contractions in avian myocytes and reinforces the connection between structural organization of the myocyte, the CRUs, and the strength and rate of cardiac contraction across vertebrate classes.

Competing interests

We have no competing interests.

Author Contributions

TS, CP, and HS designed the experimental study. TS carried out the experiments, imaging, and analysed data. CP assisted in data analysis. SRK constructed the model, incorporated the experimental data, designed, and performed the simulations. All authors contributed to interpretation of the simulation results, writing the manuscript and approved the final version.

Acknowledgements

The authors wish to thank the staff in the Faculty EM Facility for their assistance, in particular Tobias Starborg and Samantha Forbes, and the Wellcome Trust for equipment grant support to the EM Facility. We also thank Ben Newman for tissue samples, Dr Jonathan Codd for assistance with the birds, and Drs Katharine Dibb and Ashraf Kitmitto for useful discussions.

Funding

HS, CP and TS were supported by The University of Manchester. We thank Compute Canada and SharcNET Canada for computing resources to SRK.

References

AKESTER, A. R. 1981. Intercalated discs, nexuses, sarcoplasmic reticulum and transitional cells in the heart of the adult domestic fowl (Gallus gallus domesticus). *J Anat,* 133**,** 161-79.

ASGHARI, P., SCHULSON, M., SCRIVEN, D. R. L., MARTENS, G. & MOORE, E. D. W. 2009. Axial Tubules of Rat Ventricular Myocytes Form Multiple Junctions with the Sarcoplasmic Reticulum. *Biophysical Journal,* 96**,** 4651-4660.

ASGHARI, P., SCRIVEN, D. R. L., SANATANI, S., GANDHI, S. K., CAMPBELL, A. I. M. & MOORE, E. D. W. 2014. Nonuniform and Variable Arrangements of Ryanodine Receptors Within Mammalian Ventricular Couplons. *Circulation Research,* 115**,** 252-262.

BADDELEY, D., JAYASINGHE, I. D., LAM, L., ROSSBERGER, S., CANNELL, M. B. & SOELLER, C. 2009. Optical single-channel resolution imaging of the ryanodine receptor distribution in rat cardiac myocytes. *Proceedings of the National Academy of Sciences,* 106**,** 22275-22280.

BERS, D. M. 2002. Cardiac excitation-contraction coupling. *Nature,* 415**,** 198-205.

BOGDANOV, K. Y., ZIMAN, B. D., SPURGEON, H. A. & LAKATTA, E. G. 1995. L- and T-type calcium currents differ in finch and rat ventricular cardiomyocytes. *J Mol Cell Cardiol,* 27**,** 2581-93.

BOYDEN, P. A., PU, J., PINTO, J. & TER KEURS, H. E. D. J. 2000. Ca(2+) Transients and Ca(2+) Waves in Purkinje Cells Role in Action Potential Initiation. *Circulation research,* 86**,** 448-455.

CANNELL, M. B., CHENG, H. & LEDERER, W. J. 1995. The control of calcium release in heart muscle. *Science,* 268**,** 1045-9.

CHEN-IZU, Y., MCCULLE, S. L., WARD, C. W., SOELLER, C., ALLEN, B. M., RABANG, C., CANNELL, M. B., BALKE, C. W. & IZU, L. T. 2006. Three-dimensional distribution of ryanodine receptor clusters in cardiac myocytes. *Biophys J,* 91**,** 1-13.

CHENG, H., LEDERER, W. J. & CANNELL, M. B. 1993. Calcium sparks: elementary events underlying excitation-contraction coupling in heart muscle. *Science,* 262**,** 740-4.

DEERINCK, T. J., BUSHONG, E., THOR, A. & ELLISMAN, M. H. 2010. NCMIR methods for 3D EM: a new protocol for preparation of biological specimens for serial block face scanning electron microscopy.

DIBB, K. M., CLARKE, J. D., HORN, M. A., RICHARDS, M. A., GRAHAM, H. K., EISNER, D. A. & TRAFFORD, A. W. 2009. Characterization of an extensive transverse tubular network in sheep atrial myocytes and its depletion in heart failure. *Circ Heart Fail,* 2**,** 482-9.

DZIALOWSKI, E. M. & CROSSLEY II, D. A. 2015. Chapter 11 - The Cardiovascular System. *In:* SCANES, C. G. (ed.) *Sturkie's Avian Physiology (Sixth Edition).* San Diego: Academic Press.

FARRELL, A. P. 1991. From Hagfish to Tuna: A Perspective on Cardiac Function in Fish. *Physiological Zoology,* 64**,** 1137-1164.

FRANZINI-ARMSTRONG, C., PROTASI, F. & RAMESH, V. 1999. Shape, size, and distribution of Ca(2+) release units and couplons in skeletal and cardiac muscles. *Biophysical Journal,* 77**,** 1528-1539.

FRANZINI-ARMSTRONG, C., PROTASI, F. & TIJSKENS, P. 2005. The assembly of calcium release units in cardiac muscle. *Ann N Y Acad Sci,* 1047**,** 76-85.

HAYASHI, T., MARTONE, M. E., YU, Z., THOR, A., DOI, M., HOLST, M. J., ELLISMAN, M. H. & HOSHIJIMA, M. 2009. Three-dimensional electron microscopy reveals new details of membrane systems for Ca2+ signaling in the heart. *J Cell Sci,* 122**,** 1005-13.

IZU, L. T., WIER, W. G. & BALKE, C. W. 2001. Evolution of cardiac calcium waves from stochastic calcium sparks. *Biophys J,* 80**,** 103-20.

IZU, L. T., XIE, Y., SATO, D., BÁNYÁSZ, T. & CHEN-IZU, Y. 2013. Ca(2+) waves in the heart. *Journal of molecular and cellular cardiology,* 58**,** 118-124.

JUNKER, J., SOMMER, J. R., SAR, M. & MEISSNER, G. 1994. Extended junctional sarcoplasmic reticulum of avian cardiac muscle contains functional ryanodine receptors. *J Biol Chem,* 269**,** 1627-34.

KHARCHE, S. R., VIGMOND, E., EFIMOV, I. R. & DOBRZYNSKI, H. 2017. Computational assessment of the functional role of sinoatrial node exit pathways in the human heart. *PLoS One,* 12**,** e0183727.

KIM, C. S., DOYE, A. A., GWATHMEY, J. K., DAVIDOFF, A. J. & MAKI, T. M. 2000. Intracellular calcium and the relationship to contractility in an avian model of heart failure. *Journal of comparative physiology. B, Biochemical, systemic, and environmental physiology,* 170**,** 295-306.

KREMER, J. R., MASTRONARDE, D. N. & MCINTOSH, J. R. 1996. Computer visualization of three-dimensional image data using IMOD. *J Struct Biol,* 116**,** 71-6.

LOUCH, W. E., KOIVUMAKI, J. T. & TAVI, P. 2015. Calcium signalling in developing cardiomyocytes: implications for model systems and disease. *J Physiol,* 593**,** 1047-63.

MIRSALIMI, S. M., O'BRIEN, P. J. & JULIAN, R. J. 1993. Blood volume increase in salt-induced pulmonary hypertension, heart failure and ascites in broiler and White Leghorn chickens. *Canadian Journal of Veterinary Research,* 57**,** 110-113.

PERNI, S., IYER, V. R. & FRANZINI-ARMSTRONG, C. 2012. Ultrastructure of cardiac muscle in reptiles and birds: optimizing and/or reducing the probability of transmission between calcium release units. *J Muscle Res Cell Motil,* 33**,** 145-52.

PROSHEVA, V., DERNOVOJ, B., KHARIN, S., KASEVA, N., SHKLYAR, T. & BLYAKHMAN, F. 2015. Does the right muscular atrioventricular valve in the avian heart perform two functions? *Comparative Biochemistry and Physiology Part A: Molecular & Integrative Physiology,* 184**,** 41-45.

QU, Z., HU, G., GARFINKEL, A. & WEISS, J. N. 2014. Nonlinear and Stochastic Dynamics in the Heart. *Phys Rep,* 543**,** 61-162.

SHIELS, H. A. & GALLI, G. L. 2014. The sarcoplasmic reticulum and the evolution of the vertebrate heart. *Physiology (Bethesda),* 29**,** 456-69.

SHIELS, H. A. & WHITE, E. 2005. Temporal and spatial properties of cellular Ca2+ flux in trout ventricular myocytes. *Am J Physiol Regul Integr Comp Physiol,* 288**,** R1756-66.

SMITH, G. D., KEIZER, J. E., STERN, M. D., LEDERER, W. J. & CHENG, H. 1998. A simple numerical model of calcium spark formation and detection in cardiac myocytes. *Biophysical journal,* 75**,** 15-32.

SOBIE, E. A., DILLY, K. W., DOS SANTOS CRUZ, J., LEDERER, W. J. & JAFRI, M. S. 2002. Termination of cardiac Ca(2+) sparks: an investigative mathematical model of calcium-induced calcium release. *Biophysical Journal,* 83**,** 59-78.

SOBIE, E. A., GUATIMOSIM, S., GÓMEZ-VIQUEZ, L., SONG, L.-S., HARTMANN, H., JAFRI, M. S. & LEDERER, W. J. 2006. The Ca(2+) leak paradox and "rogue ryanodine receptors": SR Ca(2+) efflux theory and practice. *Progress in biophysics and molecular biology,* 90**,** 172-185.

SOMMER, J. & JOHNSON, E. 1969. Cardiac muscle. *Zeitschrift für Zellforschung und Mikroskopische Anatomie,* 98**,** 437-468.

SOMMER, J. R. 1995. Comparative anatomy: in praise of a powerful approach to elucidate mechanisms translating cardiac excitation into purposeful contraction. *J Mol Cell Cardiol,* 27**,** 19-35.

STERN, M. D., RÍOS, E. & MALTSEV, V. A. 2013. Life and death of a cardiac calcium spark. *The Journal of General Physiology,* 142**,** 257-274.

STUYVERS, B. D., DUN, W., MATKOVICH, S., SORRENTINO, V., BOYDEN, P. A. & TER KEURS, H. E. D. J. 2005. Ca2+ Sparks and Waves in Canine Purkinje Cells: A Triple Layered System of Ca2+ Activation. *Circulation Research,* 97**,** 35-43.

WOO, S.-H., CLEEMANN, L. & MORAD, M. 2003. Spatiotemporal Characteristics of Junctional and Nonjunctional Focal Ca2+ Release in Rat Atrial Myocytes. *Circulation Research,* 92**,** e1-e11.

Figures

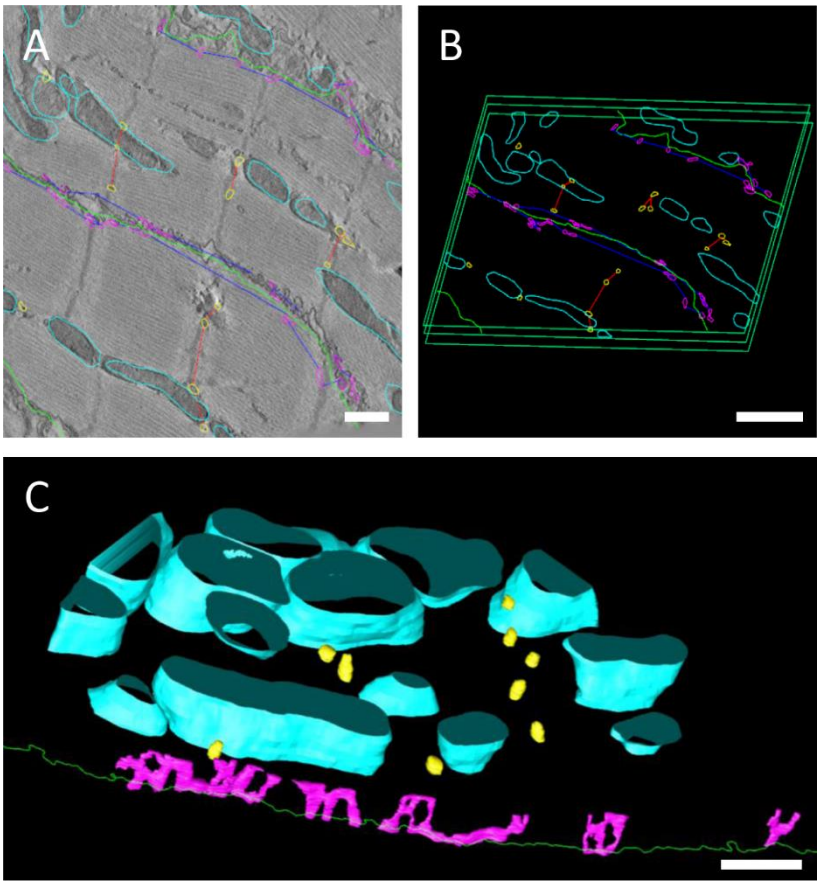

Fig. 1. Tomograms and segmented structural models used for measuring inter-CRU distances in avian left atrial tissue. **(A)** 2D image from a reconstructed tomogram stack, with a segmented model overlaid. The segmented model shows: peripheral couplings (PCs) (purple) and the nearest edge-edge distances between PCs (blue lines); corbular sarcoplasmic reticulum (cSR) (yellow) and the nearest edge-edge distances between these CRUs along a Z-line (red lines). Also segmented are the mitochondria (cyan) and the sarcolemma (green lines). Scale bar = 500 nm. Note that the segmentation overlay is from a deeper region of the tomogram than the EM image which is why the lines of the segmentation and the overlay do not always align. **(B)** 3D segmented model. The reconstruction is approximately 400 nm thick. Scale bar = 1000 nm. **(C)** 3D model showing the distribution of cSR (yellow), the peripheral SR (purple) containing PCs near the sarcolemma (green line, only segmented in a single plane). Sub-sarcolemmal mitochondria are also shown (cyan). The free SR throughout the cell that connects PCs to the cSR has also not been segmented. Scale bar = 500 nm; scale in z-plane is approximately 400 nm.

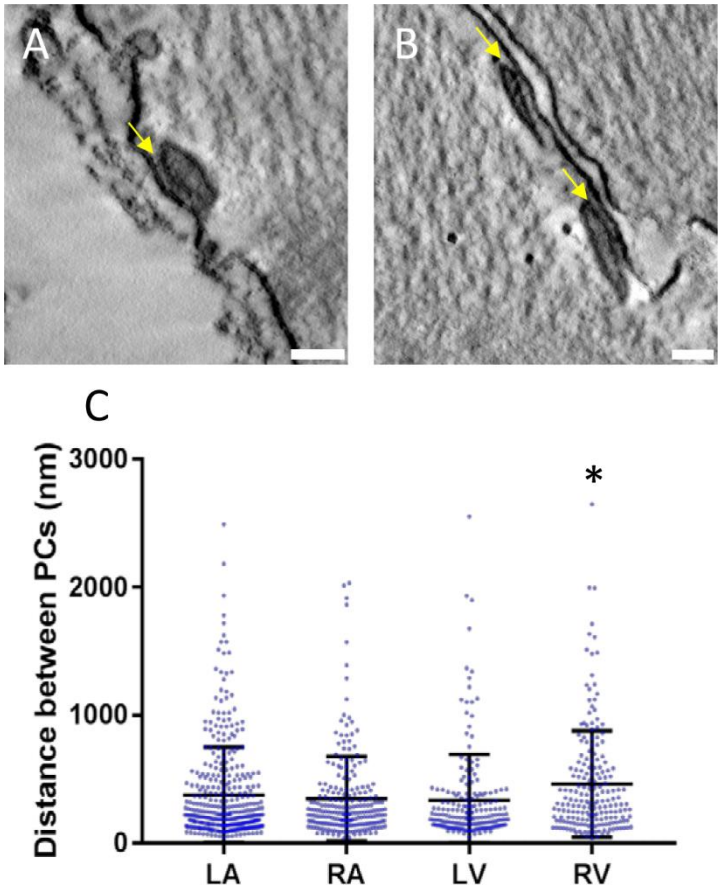

Fig. 2. Peripheral couplings (PCs) and inter PC distances in the avian right ventricle. **(A, B)** Examples of PCs (arrows) from tomograms identified as darkly stained SR cisternae that are closely opposed to the sarcolemma. Scale bars = 50 nm in both panels. **(C)** The nearest edge-edge distances between PCs in all four cardiac chambers. Scatter plots represent combined measurements for two birds (LV, RV) or three birds (LA, RA) with mean ± s.e.m. overlaid. The * signifies that the RV was statistically different to LA, RA, and LV via one-way ANOVA, with $P<0.05$. The number of distance measurements between individual PCs are as follows: n = LA (380), RA (228), LV (193), RV (195).

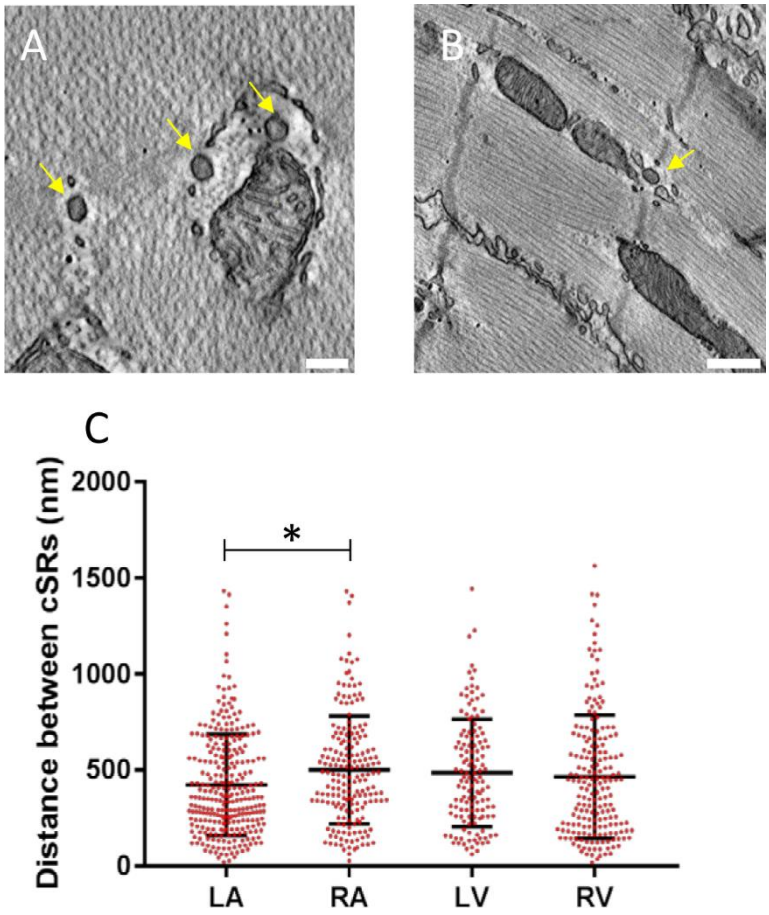

Fig. 3. Corbular sarcoplasmic reticulum (cSR) in avian cardiomyocytes. **(A, B)** Examples of cSR (arrows) from tomograms from right ventricle (A, scale bar = 100 nm**)** and left atrium (B, scale bar = 200 nm**)**, identified as darkly stained SR cisternae found near Z-lines, roughly 100 nm in width. **(C)** The nearest edge-edge distances between cSR along the same Z-line in all four cardiac chambers. Scatter plots represent combined measurements for two birds (LV, RV) or three birds (LA, RA), with mean ± s.e.m. overlaid. The * signifies that the LA was statistically different to RA (one-way ANOVA $P<0.05$). The number of distance measurements between cSR are as follows: n= LA (286), RA (189), LV (133), RV (194).

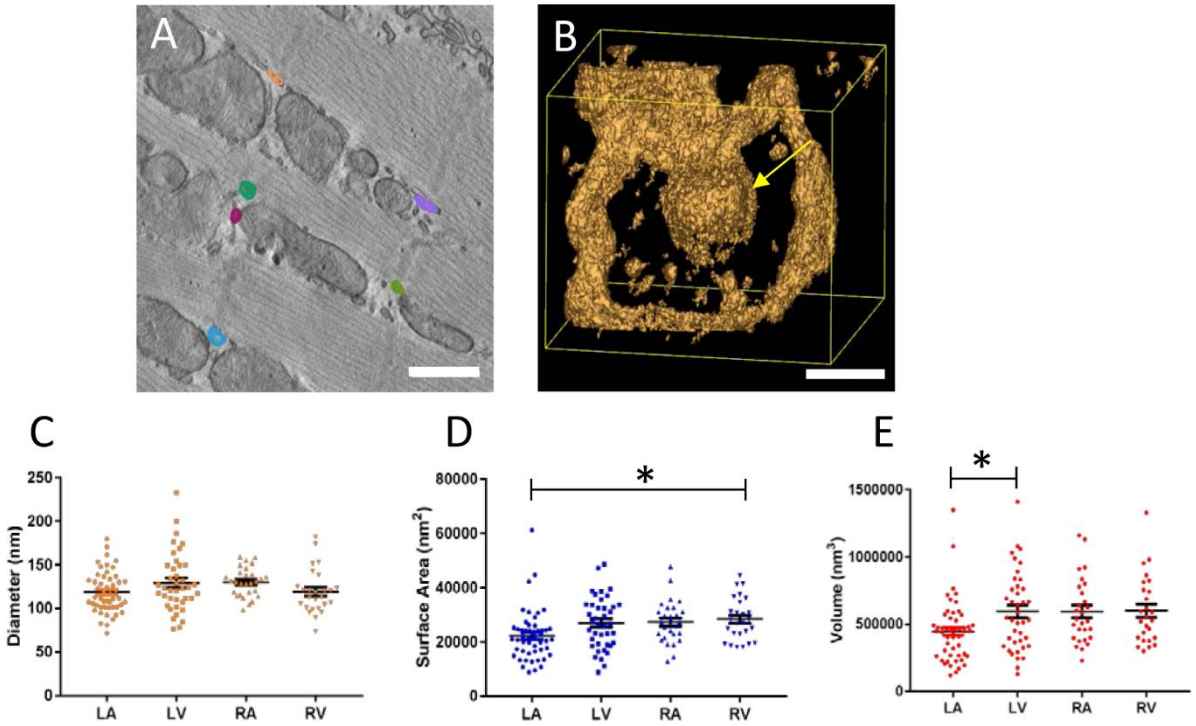

Fig. 4. Geometric models of the corbular sarcoplasmic reticulum (cSR) in avian myocardium. **(A)** 3D segmented cSR (various colours). Scale bar = 1000 nm. **(B)** Isosurface rendering of an individual cSR (arrow), attached to the free SR network. Scale bar = 100 nm. Scatterplots show the spread of the data for **(C)** diameter, **(D)** surface area and **(E)** volume of individual cSR, in the 4 chambers of the heart with mean ± s.e.m. overlaid. The same data is tabulated in Table S2. Measurements were performed in all 4 chambers from a bird heart; n= LA (50), RA (40), LV (28), RV (26). Statistical analyses showed LA statistically different to RV in (D) and LA statistically different to LV in (E).

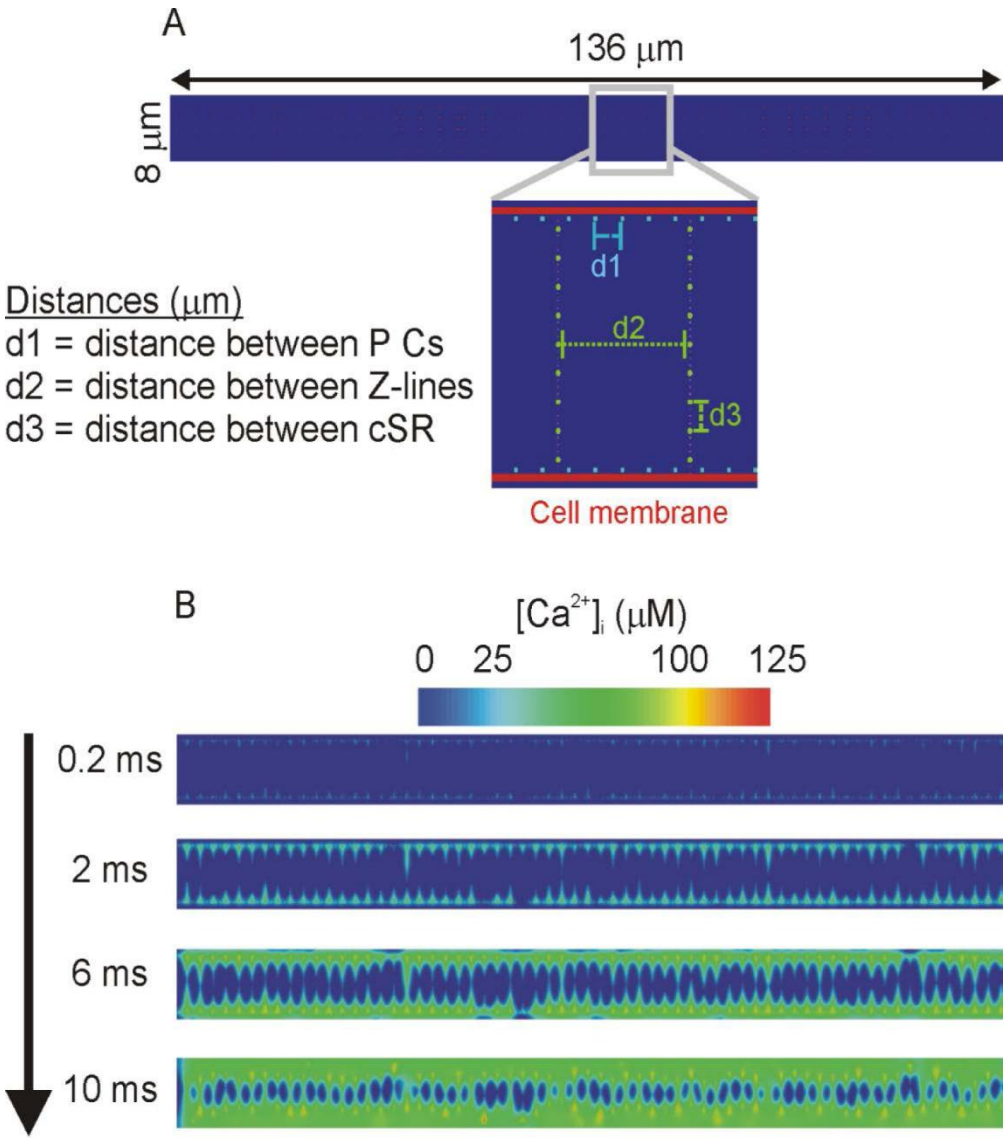

Fig. 5. Simulated cell activation time and direction of Ca^{2+} wave propagation. **(A)** 2D model geometry showing distance between CRUs. **(B)** Representative frames from a simulation of Ca^{2+} waves. Top panel shows stimulation at cell membrane. In the middle and bottom panels, Ca^{2+} diffuses from Ca^{2+} release sites to neighbouring sites and induces Ca^{2+} release at the neighbouring sites leading to whole cell Ca^{2+} activation.

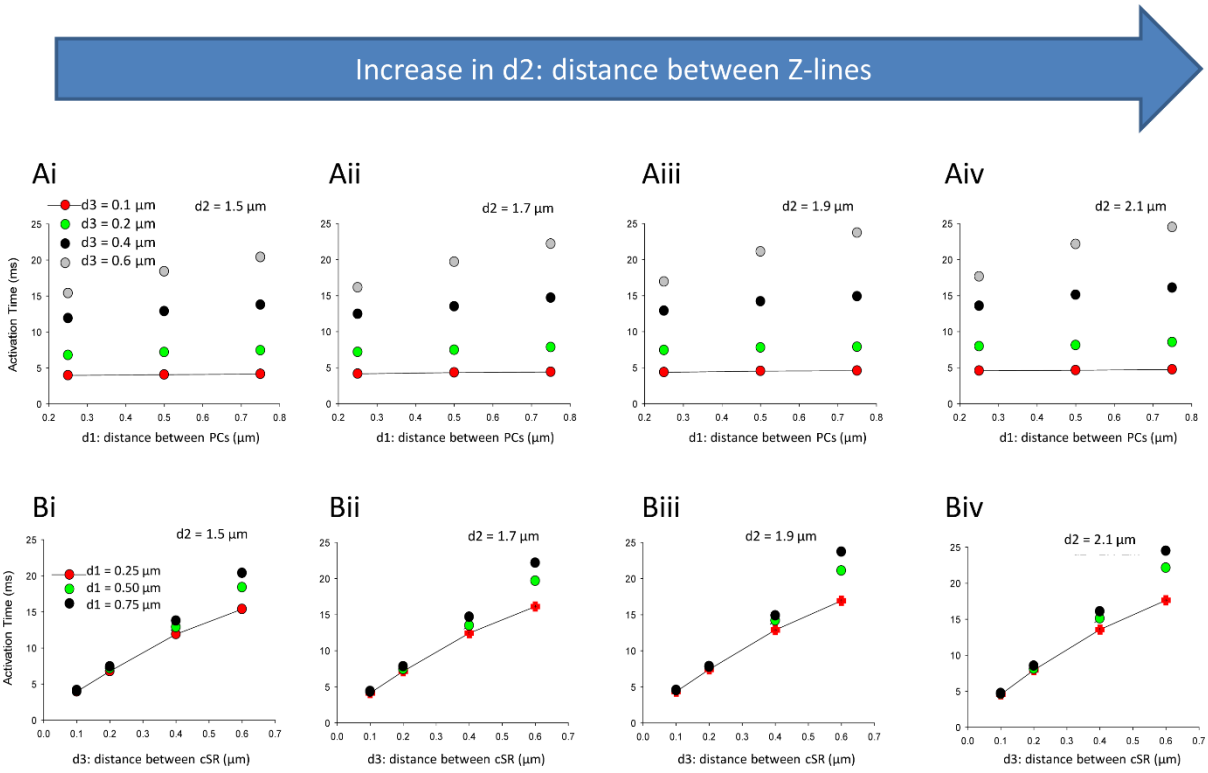

Fig. 6. Output of 2D avian cell model showing activation times (ms) as a function of d1, distance between PCs **(A)**; and d3, distance between cSR along a Z-line **(B)**. Within each panel (i-iv) the relationship is plotted as d2 (distance between Z-lines) is increased. The distance of d2 was varied to represent Z-line spacing indicative of a myocyte at rest (1.7- 1.9 µm), as well as encompassing values that could be achieved during myocardial stretch (2.1 µm) and during myocardial contraction (1.5 µm). In each graph, the circles represent the averaged result of 10 simulations. Each simulation required 24 processors for 4 hours.

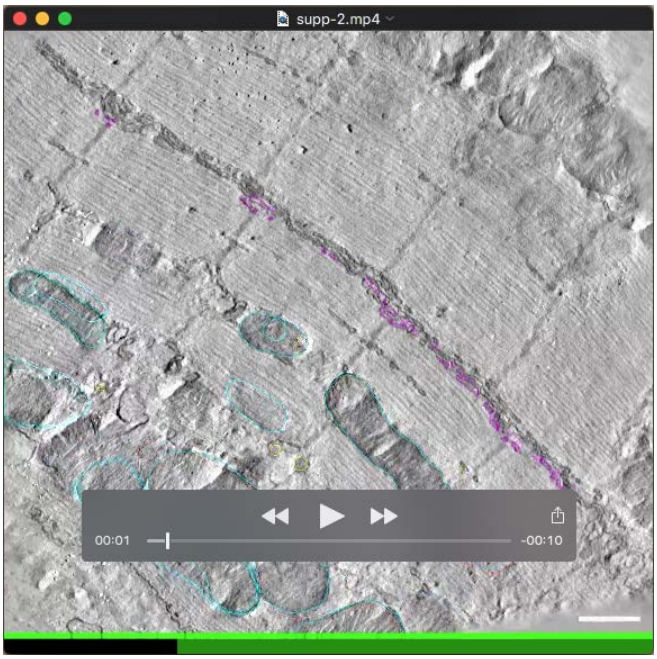

Movie 1. Tomogram in the avian left atrium, as in Figure 1A. The tomogram was segmented for cSR (yellow), mitochondria (cyan), and the SR network (purple) adjacent to the sarcolemma (green line), in order to obtain the 3D model shown in Figure 1C and Supplementary Video 2. Scale bar = 500 nm.

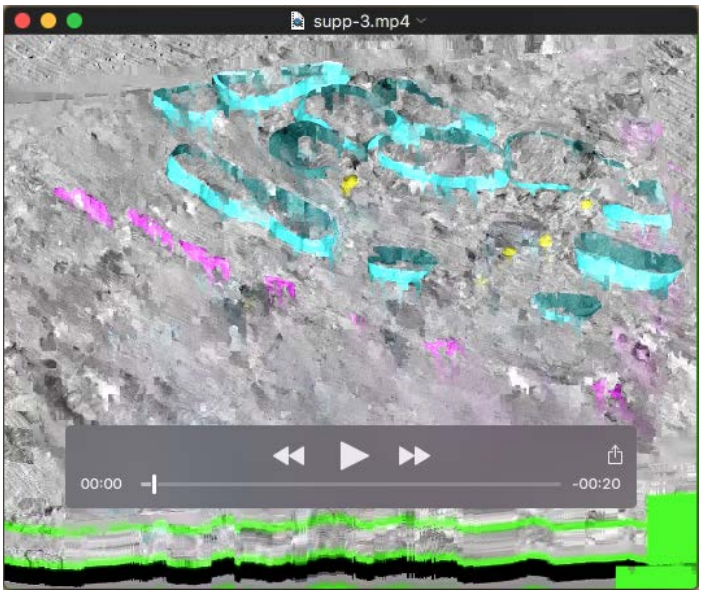

Movie 2. Segmented 3D model of avian left atrium, as in Figure 1C. Segmented are the cSR (yellow), mitochondria (cyan), and the SR network (purple) adjacent to the sarcolemma (green line). Scale bar = 1000 nm.

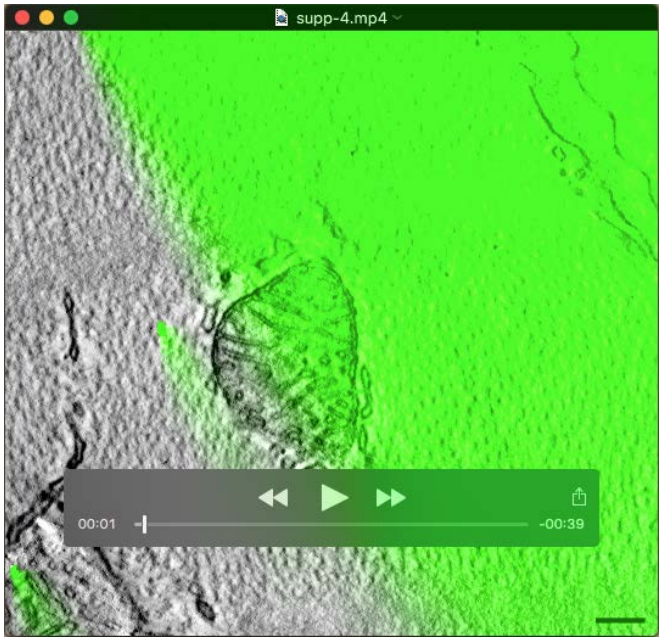

Movie 3. cSR in the avian right ventricle. Scale bar = 200 nm.

Table S1. Modelling parameters used in the equations (see methods) to simulate results obtained in Figures 5 and 6.

Parameter symbol and description	Mammalian value	Avian value	Units
***Morphology*[1]**			
D, Diameter of cell	8	8.7	µm
L, Length of cell	104	136	µm
d_1, Distance between PCs,		0.25, 0.5, 0.75	
d_2, Distance between consecutive Z disks	1.8	1.5, 1.7, 1.9, 2.1	µm
d_3, Distance between cSR within a Z disk	0.4	0.1, 0.2, 0.4, 0.6	µm
***Reactions*[2]**			
D_c, diffusion constant of cytosolic Ca^{2+}	0.25	0.25	$\mu m^2/ms$
$[B_n]$ total, maximum immobile buffer CMDN	123	123	µM
K_n^+	0.1	0.1	µM/ms
K_n^-	0.1	0.1	/ms
$V_{max,pump}$	0.208	0.208	µM/ms
M	3.98	3.98	No units
K_{pump}	0.184	0.184	µM
c_∞	0.1	0.1	µM
K, Ca^{2+} release threshold	15	15	µM
Ta, time duration when RyR releases Ca^{2+} from SR to cytosol	10	10	ms

A, max. amplitude of local Ca^{2+} release	15	15	μM
Finite difference scheme parameters			
dx, space step	0.05	0.05	μm
dt, time step	0.02	0.02 (adaptive time step)	ms

[1] Morphology was based on (Kim *et al.*, 2000). [2]Reactions were based on (Cheng *et al.*, 1993; Izu *et al.*, 2001).

Table S2. Summary of individual cSR geometric and volumetric data for the four chambers of avian myocardium.

	Left Atrium	**Left Ventricle**	**Right Atrium**	**Right Ventricle**
cSR diameter (nm)	119±3	129±5	130±3	119±5
cSR surface area (nm^2)	22262±1315*	26972±1510	27370±1470	28401±1530*
cSR volume (nm^3)	446249±32357*	593937±45955*	593673±45450	600288±49132

Data are presented as mean±SEM. Measurements of corbular SR (cSR) were performed in all 4 chambers from a single bird heart; n measurements = LA (50), RA (40), LV (28), RV (26). Paired * indicates significant differences (one-way ANOVA, $P<0.05$) within a measurement.

References

CHENG, H., LEDERER, W. J. & CANNELL, M. B. 1993. Calcium sparks: elementary events underlying excitation-contraction coupling in heart muscle. *Science,* 262**,** 740-4.

IZU, L. T., WIER, W. G. & BALKE, C. W. 2001. Evolution of cardiac calcium waves from stochastic calcium sparks. *Biophys J,* 80**,** 103-20.

KIM, C. S., DOYE, A. A., GWATHMEY, J. K., DAVIDOFF, A. J. & MAKI, T. M. 2000. Intracellular calcium and the relationship to contractility in an avian model of heart failure. *Journal of comparative physiology. B, Biochemical, systemic, and environmental physiology,* 170**,** 295-306.